

---

# Representation Reliability and Its Impact on Downstream Tasks

---

Young-Jin Park<sup>1</sup>, Hao Wang<sup>2</sup>, Shervin Ardeshtir, and Navid Azizan<sup>1</sup>

<sup>1</sup>Massachusetts Institute of Technology

<sup>2</sup>MIT-IBM Watson AI Lab

youngjp@mit.edu, hao@ibm.com, shervin.ardeshir@gmail.com, azizan@mit.edu

## Abstract

Self-supervised pre-trained models extract general-purpose representations from data, and quantifying how reliable they are is crucial because many downstream models use these representations as input for their own tasks. To this end, we first introduce a formal definition of *representation reliability*: the representation for a given test input is considered to be reliable if the downstream models built on top of that representation can consistently generate accurate predictions for that test point. It is desired to estimate the representation reliability without knowing the downstream tasks a priori. We provide a negative result showing that existing frameworks for uncertainty quantification in supervised learning are not suitable for this purpose. As an alternative, we propose an ensemble-based method for quantifying representation reliability, based on the concept of *neighborhood consistency* in the representation spaces across various pre-trained models. More specifically, the key insight is to use shared neighboring points as anchors to align different representation spaces. We demonstrate through comprehensive numerical experiments that our method is capable of predicting representation reliability with high accuracy.

## 1 Introduction

Self-supervised learning has opened the door to the development of general-purpose embedding functions, often referred to as *foundation models*, that can be used or fine-tuned for various downstream tasks (Jaiswal et al., 2020; Jing and Tian, 2020). These embedding functions are pre-trained on large corpora of different data modalities, spanning visual (Chen et al., 2020a), textual (Brown et al., 2020), audio (Al-Tahan and Mohsenzadeh, 2021), and their combinations (Radford et al., 2021; Morgado et al., 2021), aimed at being general purpose and agnostic to the downstream tasks they may be utilized for. For instance, the recent surge in large pre-trained models such as CLIP (Radford et al., 2021) and ChatGPT (OpenAI, 2022) has resulted in the development of many prompt-based or dialogue-based downstream use cases, none of which are known a priori when the pre-trained model is being deployed.

Embedding functions learned through self-supervised learning do not always produce reliable outputs. For example, large language models can generate factually inaccurate information with a high level of confidence (Bommasani et al., 2021; Tran et al., 2022). With the increasing use of self-supervised learning to generate textual, visual, and audio content, unreliable embedding functions could have significant implications. Furthermore, given that these embedding functions are frequently employed as frozen backbones for various downstream use cases, adding more labeled downstream data may not improve the performance if the initial representation is unreliable. Therefore, *having notion(s) of reliability/uncertainty for such pre-trained models alongside their abstract embeddings would be a key enabler for their reliable deployment, especially in safety-critical settings.*

In this paper, we introduce a formal definition of representation reliability based on its impact on downstream tasks. Our definition pertains to a representation of a given test point produced by a pre-trained embedding function. If a variety of downstream tasks that build upon this representation consistently yield accurate results for the test point, we consider this representation reliable. Existing uncertainty quantification frameworks mostly focus on the supervised learning setting, where they rely on the consistency of predictions across various predictive models. We provide a counter-example showing that they cannot be directly applied to our context, as representations lack a ground truth for comparison. In other words, inconsistent predictions often indicate a high prediction uncertainty, but inconsistent representations do not necessarily imply unreliable representations. Hence, it is critical to align representation spaces in such a way that corresponding regions have consistent semantic meanings before comparing them.

To this end, we propose an ensemble-based approach for estimating representation reliability. We prove that a test point has a reliable representation if it has a reliable neighbor which remains consistently close to the test point, across multiple representation spaces generated by different embedding functions. Based on this theoretical insight, we select a set of embedding functions and reference data (e.g., data used for training the embedding functions). We then compute the number of consistent neighboring points in the reference data to estimate the representation reliability. The underlying reasoning is that a test point with more consistent neighbors is more likely to have a reliable and consistent neighbor. This reliable and consistent neighbor can be used to align different representation spaces that are generated by different embedding functions.

We conduct extensive numerical experiments to validate our approach and compare it with state-of-the-art out-of-distribution (OOD) detection measures. The results indicate that our approach consistently captures the reliability of representations and outperforms the baselines in terms of correlation with representation reliability. Moreover, we observe that our approach is more robust than the baselines with respect to the geometry of the representation space. Specifically, regardless of using Euclidean or cosine distance to compute consistent neighboring points, our approach shows a high correlation with representation reliability. On the other hand, the choice of distance measures significantly impacts the performance of baseline approaches and can even result in a negative correlation with representation reliability.

In summary, our main contributions are:

- We present a formal definition of representation reliability, which is measured by its impact on various downstream tasks. To the best of our knowledge, this is the first comprehensive study to investigate uncertainty in representation space.
- We provide a counter-example, showing that existing supervised learning frameworks for studying uncertainty cannot be directly applied to estimate representation reliability.
- We prove that identifying an anchor point that aligns various representation spaces is crucial in estimating representation reliability.
- Based on our theoretical findings, we introduce an ensemble-based approach that uses neighborhood consistency to measure representation reliability.
- We conduct comprehensive numerical experiments, showing that our metric can consistently capture representation reliability and outperforms baseline methods.

## Related Works

**Uncertainty Quantification in Supervised Learning.** Existing work on uncertainty quantification mostly focused on supervised learning settings. For example, Bayesian inference quantifies uncertainty by placing a prior distribution over model parameters, updating this prior distribution with observed data to obtain a posterior distribution, and examining the inconsistency of predictions derived from the posterior distribution (Neal, 1996; MacKay, 1992; Kendall and Gal, 2017; Depeweg et al., 2018). Since the posterior distribution may not have an analytical form, many approximating approaches have been introduced, including Monte Carlo dropout (Gal and Ghahramani, 2016), deep ensembles (Osband et al., 2018; Lakshminarayanan et al., 2017; Wen et al., 2020), and Laplace approximation (Daxberger et al., 2021; Sharma et al., 2021). In this paper, we focus on quantifying the uncertainty of representations and prove that standard supervised-learning frameworks cannot be directly applied to investigate representation uncertainty (see Section 3.2 for more details).

**Novelty Detection and Representation Reliability.** Self-supervised learning is increasingly used for out-of-distribution (OOD) detection. This approach involves training an embedding function and then computing an OOD score for a new test point based on its distance from the training data in the representation space (Lee et al., 2018; van Amersfoort et al., 2020; Tack et al., 2020; Mirzae et al., 2022). It is important to note that representation reliability and OOD detection are different concepts. Being in-distribution does not necessarily guarantee the reliability of a sample’s representation, and vice versa. Recently, Ardeshir and Azizan (2022) introduced several empirical measures for quantifying representation uncertainty. To compare with this line of work, we conduct comprehensive numerical experiments (Section 4). The results suggest that our approach is more favorably correlated with the representation reliability compared with state-of-the-art OOD detection measures and the empirical metrics proposed in Ardeshir and Azizan (2022).

**Uncertainty-aware Representation Learning.** There is a growing body of research aimed at training robust self-supervised models using an embedding function that maps input points to distribution in the representation space as opposed to a single point (Vilnis and McCallum, 2015; Neelakantan et al., 2015; Karaletsos et al., 2015; Bojchevski and Günnemann, 2017; Oh et al., 2018; Chen et al., 2020a; Wu and Goodman, 2020; Zhang et al., 2021). These methods modify the neural network’s architecture and introduce alternative training schemes. For example, the approach proposed by Zhang et al. (2021) requires an additional output (i.e., a temperature parameter), while the approach by Oh et al. (2018) necessitates the network to output means and variances of a mixture of Gaussian distributions. However, these methods primarily focus on the training scheme and adopt relatively simple (and heuristic) approaches for quantifying uncertainty. In contrast, we aim to avoid making any assumptions about the training process of the embedding function, while only necessitating black-box access to it. Furthermore, we provide a theoretical analysis of our method and explore the impact of representation reliability on the performance of downstream tasks.

We provide a more in-depth discussion about related works in Appendix E.

## 2 Background: Uncertainty Quantification in Supervised Learning

We recall a Bayesian-inference view of uncertainty in supervised learning. Consider a class of predictive models  $\mathcal{F}$ , where each model  $f$  generates a predictive probability  $p(y|\mathbf{x}, f)$  for an input variable  $\mathbf{x}$ . In the Bayesian framework, a prior probability distribution  $p(f)$  is first introduced over  $\mathcal{F}$  and a posterior distribution is learned given a training dataset  $\mathcal{D}$ :  $p(f|\mathcal{D}) \propto p(\mathcal{D}|f) \cdot p(f)$ . For a new test point  $\mathbf{x}^*$ , its posterior predictive distribution is obtained by averaging the predictive probabilities over models:

$$p(\hat{y}^*|\mathbf{x}^*, \mathcal{D}) = \int p(\hat{y}^*|\mathbf{x}^*, f)p(f|\mathcal{D})df. \quad (1)$$

Since the posterior distribution does not have an analytical expression for complex neural networks, Monte Carlo approaches are often used to approximate (1). A special instance is deep ensembles (Lakshminarayanan et al., 2017) that train a set of neural networks with different random initialization of the learnable parameters  $\{\theta_i\}_{i=1}^M$ . Assume a uniform prior over functions and sampling models well-fitted to  $\mathcal{D}$  (i.e., treating the likelihood of different models as equal and dominant), the posterior predictive distribution can be approximated by

$$p(\hat{y}^*|\mathbf{x}^*, \mathcal{D}) \approx \frac{1}{M} \sum_{i=1}^M [\delta(\hat{y}^* - f_{\theta_i}(\mathbf{x}^*))]. \quad (2)$$

Finally, the uncertainty can be assessed by the *inconsistency* (e.g., measured by variance) of the output across sampled functions:

$$U_{\text{supervised}}(\mathbf{x}^*) \triangleq \text{Var}(\hat{y}^* | \mathbf{x}^*, \mathcal{D}) \approx \text{Var}_{i \sim [M]}(f_{\theta_i}(\mathbf{x}^*)). \quad (3)$$

When different models produce significantly different predictions, it suggests a higher level of uncertainty. Conversely, if multiple independently trained models map an input variable to similar outputs, the prediction can be considered certain.

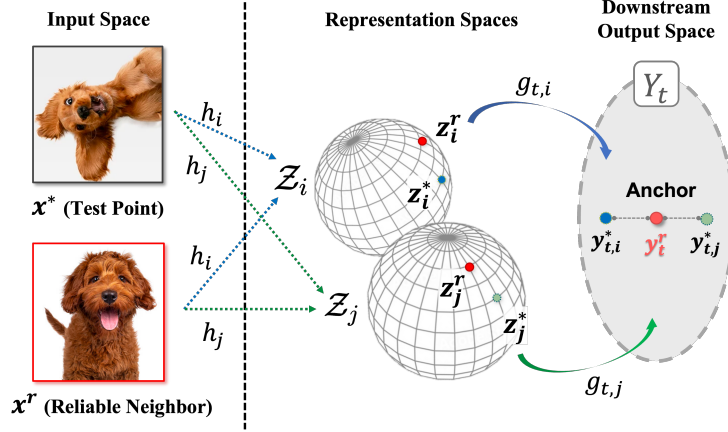


Figure 1: Illustration of our proposed method. Let  $\mathcal{Z}_i$  and  $\mathcal{Z}_j$  be representation spaces determined by embedding function  $h_i$  and  $h_j$ . For a downstream task  $t$ , a reliable neighboring point  $x^r$  serves as an anchor for comparing different representations  $z_i^* = h_i(x^*)$  and  $z_j^* = h_j(x^*)$  of the test point  $x^*$ .

### 3 Estimating Representation Reliability

In this section, we introduce a formal definition of representation reliability by examining its impact on downstream tasks. We provide a negative result showing that existing supervised learning uncertainty quantification frameworks (described in Section 2) are inadequate for capturing representation reliability. We present an ensemble-based method that examines the consistency of neighboring points in the representation space. Numerical experiments show that our method consistently exhibits a high correlation with representation reliability.

#### 3.1 Representation Reliability

Consider an embedding function  $h : \mathcal{X} \rightarrow \mathcal{Z}$  that maps a data point (e.g., an image) to the representation space  $\mathcal{Z}$ . Here the representation space can be either a real- $d$  space  $\mathbb{R}^d$  or a unit hypersphere  $S^{d-1}$ . Below, we provide a formal definition of *representation reliability* by analyzing its impact on a collection of downstream tasks. Intuitively, a reliable representation should consistently lead to more accurate results across these downstream tasks.

**Definition 1.** Suppose there is a collection of downstream prediction tasks  $\mathcal{T}$ . Each task builds upon a common embedding function  $h$  and learns a predictive model  $g_t \circ h : \mathcal{X} \rightarrow \mathcal{Y}_t$ . The representation reliability for a given test point  $x^* \in \mathcal{X}$  is defined as

$$\text{Reli}(x^*; h) \triangleq \mathbb{E}_{t \sim \mathcal{T}} [\text{Perf}(g_t \circ h(x^*), y_t^*)] \quad (4)$$

where  $y_t^* \in \mathcal{Y}_t$  denotes the ground-truth label of  $x^*$  under task  $t$ , Perf is a performance metric (e.g., accuracy or variance of predictive outputs), and the expectation is taken over downstream task  $t$  chosen uniformly at random from  $\mathcal{T}$ .

The above definition assumes that the set of downstream tasks and ground-truth labels are accessible. However, it is important to note that in practical scenarios, this may not always be the case. Next, we discuss how to estimate the representation reliability solely based on the properties of the representations themselves, without relying on access to the downstream labels.

#### 3.2 First Attempt: Representation Consistency

Our first attempt is directly applying standard supervised-learning techniques (see Section 2) to estimate representation reliability. Recall that if multiple predictive models give different predictions for the same test point, then it is likely that their predictions are uncertain. One may wonder if they could apply the same idea to estimate representation reliability. We present a negative result, showing that even if different embedding functions produce completely different representations, their downstream predictions can still be consistent.

**Theorem 1.** Suppose the representation reliability in Definition 1 is evaluated via downstream regression tasks. Each task builds upon an embedding function  $h_i$  and applies the empirical risk minimization to find an optimal linear head  $g_{i,t}$ . For any given  $A > 0$ , there exists a set of embedding functions  $h_1, \dots, h_M$  such that  $\text{Var}_{i \sim [M]}(h_i(\mathbf{x}^*)) \geq A$  but  $\text{Var}_{i \sim [M]}(g_{i,t} \circ h_i(\mathbf{x}^*)) = 0$  for any downstream task  $t$ . Here  $\text{Var}_{i \sim [M]}(h_i(\mathbf{x}^*)) \triangleq \mathbb{E}_{i \sim [M]}[\|h_i(\mathbf{x}^*) - \mathbb{E}_{i' \sim [M]}[h_{i'}(\mathbf{x}^*)]\|_2^2]$ .

*Proof.* See Appendix A.1. □

The key insight behind our proof is that an input point’s representation may not be unique (e.g., rotated spaces are in fact equivalent) and there is no ground truth to compare with. In other words, even if different embedding functions assign distinct representations to the same test point, downstream heads built on these embedding functions can also vary, ultimately leading to similar predictions.

### 3.3 Proposed Method: Neighborhood Consistency

Unlike in supervised learning, where inconsistent predictions often indicate high uncertainty, having diverse embeddings does not necessarily imply that the representations are unreliable. This is because the representation space is different from the output space, and it does not have a ground truth to compare with. To address this issue, we propose the idea of using an “anchor” point to align different representation spaces. The anchor point serves as a bridge that transforms different representation spaces into the same space. We can formalize this intuition more rigorously in the following theorem. It states that if a test point has a reliable neighborhood consistently around it across all representation spaces, then its downstream predictions are certain.

**Theorem 2.** For a test point  $\mathbf{x}^*$ , suppose there exists a **reliable** and **consistent** neighbor  $\mathbf{x}^r$  across all embedding functions  $h_1, \dots, h_M$ , satisfying

$$|y_t^r - g_{i,t} \circ h_i(\mathbf{x}^r)| \leq \epsilon_r, \quad \forall i \in [M] \quad (\text{Reliability of } \mathbf{x}^r) \quad (5)$$

$$\|h_i(\mathbf{x}^r) - h_i(\mathbf{x}^*)\|_2 \leq \epsilon_{nb}, \quad \forall i \in [M] \quad (\text{Consistent neighbor}) \quad (6)$$

where  $y_t^r$  is the ground-truth label of  $\mathbf{x}^r$  under downstream task  $t$ ; and  $g_{i,t}$  is the downstream classifier built upon embedding function  $h_i$  under task  $t$ . Moreover, suppose  $g_{i,t}(\mathbf{z}) = a(\mathbf{w}_{i,t}^T \mathbf{z} + b_{i,t})$  with a normalized weight  $\|\mathbf{w}_{i,t}\|_2 = 1$  and an 1-Lipschitz continuous activation function  $a(\cdot)$  (e.g., sigmoid and identity). Then for any downstream task  $t$ :

$$\text{Var}_{i \sim [M]}(g_{i,t} \circ h_i(\mathbf{x}^*)) \leq 2 \left(1 - \frac{1}{M}\right) (\epsilon_{nb} + \epsilon_r)^2. \quad (7)$$

*Proof.* See Appendix A.3. □

The above theorem suggests that a reliable and consistent neighbor can serve as an anchor point for aligning different representation spaces (see Appendix B for more discussions). Nevertheless, in practice, identifying such a neighbor may be difficult without prior knowledge of the downstream tasks. Instead of searching for a single reliable and consistent point as the anchor, we draw a set of reference points, denoted as  $\mathbf{X}_{\text{ref}} = \{\mathbf{x}^{(l)}\}_{l=1}^n$ , which can be the pre-training data for the embedding function. We then compute the number of consistent neighboring points in  $\mathbf{X}_{\text{ref}}$  and use it to estimate the representation reliability. The rationale behind this approach is that a test point with more consistent neighbors is more likely to have a reliable and consistent neighbor. This motivates the following definition for estimating representation reliability.

**Proposed Method:** Given a set of embedding functions  $h_1, \dots, h_M$  and a reference dataset  $\mathbf{X}_{\text{ref}} = \{\mathbf{x}^{(l)}\}_{l=1}^n$ , we define **Neighborhood Consistency** (NC) of a test point  $\mathbf{x}^*$  as

$$\text{NC}_k(\mathbf{x}^*) = \frac{1}{M^2} \sum_{i < j} \text{Sim}(k\text{-NN}_i(\mathbf{x}^*), k\text{-NN}_j(\mathbf{x}^*)) \quad (8)$$

where  $k\text{-NN}_i(\mathbf{x}^*)$  is the index set of  $k$  nearest neighbors of  $h_i(\mathbf{x}^*)$  among  $\{h_i(\mathbf{x}) \mid \mathbf{x} \in \mathcal{D}_{\text{ref}}\}$ ; and  $\text{Sim}(\cdot, \cdot)$  is a measure of similarity between sets. We use *Jaccard Similarity* as the metric for set similarity  $\text{Sim}(\cdot, \cdot)$  inspired by a graph representation interpretation of our method (see Appendix C for more details).

We can use different distance metrics to find the nearest neighbors, depending on the geometry of the representation space. For example, we can use cosine distance for embeddings in a unit hyper-sphere and Euclidean distance for embeddings in real space.

The value of  $k$  involves a trade-off between incorporating more consistent neighbors and increasing the overall reliability of those neighbors. If we choose a large value of  $k$ , it is more likely to find a consistent anchor point, but this anchor point may be less reliable. Conversely, if we choose a small value of  $k$ , it may filter out a desirable anchor point but the reliability of the consistent neighbors will increase. To address this issue, we will conduct an ablation study to search for the optimal  $k$  in the next section.

## 4 Numerical Experiments

### 4.1 Experiment Setup

**Embedding function.** We use the SimCLR approach (Chen et al., 2020a) to pre-train ResNet-18 and ResNet-50 models (He et al., 2016) as the embedding functions, using a single NVIDIA V100 GPU. Moreover, we conducted our experiments on two pre-training datasets, CIFAR-10 and CIFAR-100 (Krizhevsky et al., 2009), which consist of 50,000 training points and 10,000 test points. During the pre-training stage, we did not utilize any class label information. To construct the ensemble, we trained a total of  $M = 10$  models on the same dataset with different initializations, following Lakshminarayanan et al. (2017). The code will be made available upon publication.

**Downstream task.** Recall that our definition of representation reliability (Definition 1) depends on a set of downstream tasks. To optimize the utilization of the original dataset’s multi-class labels and reduce uncertainty arising from the downstream tasks themselves, we construct a set of binary classification tasks. Specifically, we define a pre-training dataset  $\mathbf{X}_{\text{down}} = \mathbf{X}_1 \cup \dots \cup \mathbf{X}_C$ , where  $C$  denotes the total number of classes in the dataset, and  $\mathbf{X}_i$  contains the data with class label  $i$ . The set of downstream tasks  $\mathcal{T}$  is composed by binary classification tasks that determine whether a data point’s label is  $i$  or  $j$ , where  $i \neq j$  and  $i, j \in [C]$ , assuming the data belongs to  $\mathbf{X}_i \cup \mathbf{X}_j$ . As a result, the total number of tasks is  $|\mathcal{T}| = C(C - 1)/2$ , with each data point being evaluated in  $(C - 1)$  tasks. We measure the performance of each downstream task based on the accuracy score:  $\text{Perf}(\hat{y}, y) = -\log |\hat{y} - y|$ . Finally, we compute the representation reliability of a test point by averaging its values across multiple embedding functions.

**Baseline.** We compare our proposed method ( $\text{NC}_k$  in (8)) with state-of-the-art OOD detection scores and the empirical measures proposed in Ardeshir and Azizan (2022) :

- $\text{AvgDist}_k$  (Tack et al., 2020; Mirzae et al., 2022): the average of the  $k$  minimum distances from the test point to the reference data in the representation space. A lower value of  $\text{AvgDist}_k$  indicates higher reliability.
- Norm (Tack et al., 2020): the  $L_2$  norm of the representation  $\|h(\mathbf{x}^*)\|_2$ . A higher value of Norm indicates higher reliability.
- LL (Ardeshir and Azizan, 2022): the log-likelihood of the data estimated by Gaussian mixture models, trained on the reference data. A higher value of LL indicates higher reliability.
- Feature Variance (FV): representation consistency measured by  $\text{Var}_{i \sim [M]}(h_i(\mathbf{x}^*))$ , as described in Theorem 1; this measure is extended from Ardeshir and Azizan (2022) to account for ensembles. A lower value of FV indicates higher reliability.

To reduce the computational burden, we randomly select 5,000 (i.e., 10%) pre-training data as the reference dataset  $\mathcal{D}_{\text{ref}}$ . We repeat our experiments 5 times to report an error bar for each evaluation metric.

All baselines, except FV, are based on a single embedding function. For a fair comparison, we additionally consider the (point-wise) ensemble average of each score over different embedding functions for  $\text{AvgDist}_k$ , Norm, and LL. We report the best results obtained either from the scores computed individually for each function or from the ensemble average for those baseline methods.

We choose  $k = 100$  for  $\text{NC}_k$  and  $k = 1$  for  $\text{AvgDist}_k$  (see Section 4.2.2 for an ablation study about the choice of  $k$ ). For our method and  $\text{AvgDist}_k$ , we test both cosine distance and Euclidean distance



Table 1: Comparison between neighborhood consistency (ours) and baselines. The highest scores for each evaluation metric are highlighted in bold. We run our experiments for multiple trials with random selections of  $\mathcal{D}_{\text{ref}}$  and report the standard deviation. As shown, our approach exhibits a high correlation with representation reliability and consistently outperforms baselines.

| Method                      | distance / normalized | ResNet-18                |                          |                          |                          | ResNet-50                |                          |                          |                          |
|-----------------------------|-----------------------|--------------------------|--------------------------|--------------------------|--------------------------|--------------------------|--------------------------|--------------------------|--------------------------|
|                             |                       | CIFAR-10                 |                          | CIFAR-100                |                          | CIFAR-10                 |                          | CIFAR-100                |                          |
|                             |                       | PCC                      | AUROC                    | PCC                      | AUROC                    | PCC                      | AUROC                    | PCC                      | AUROC                    |
| NC <sub>100</sub><br>(Ours) | cosine                | <b>0.630</b> $\pm$ 0.008 | <b>0.787</b> $\pm$ 0.003 | <b>0.562</b> $\pm$ 0.003 | <b>0.743</b> $\pm$ 0.002 | <b>0.611</b> $\pm$ 0.010 | <b>0.772</b> $\pm$ 0.004 | <b>0.534</b> $\pm$ 0.003 | <b>0.731</b> $\pm$ 0.002 |
|                             | Euclidean             | 0.565 $\pm$ 0.007        | 0.757 $\pm$ 0.004        | 0.536 $\pm$ 0.003        | 0.730 $\pm$ 0.002        | 0.538 $\pm$ 0.005        | 0.737 $\pm$ 0.003        | 0.493 $\pm$ 0.004        | 0.712 $\pm$ 0.002        |
| AvgDist <sub>1</sub>        | cosine                | 0.457 $\pm$ 0.008        | 0.687 $\pm$ 0.005        | 0.203 $\pm$ 0.010        | 0.573 $\pm$ 0.003        | 0.463 $\pm$ 0.005        | 0.684 $\pm$ 0.003        | 0.221 $\pm$ 0.018        | 0.583 $\pm$ 0.003        |
|                             | Euclidean             | -0.252 $\pm$ 0.006       | 0.417 $\pm$ 0.004        | -0.068 $\pm$ 0.008       | 0.461 $\pm$ 0.001        | -0.234 $\pm$ 0.005       | 0.422 $\pm$ 0.001        | -0.043 $\pm$ 0.008       | 0.478 $\pm$ 0.003        |
| Norm                        | -                     | 0.470                    | 0.657                    | 0.233                    | 0.588                    | 0.449                    | 0.651                    | 0.203                    | 0.574                    |
| LL                          | normalized            | 0.350 $\pm$ 0.045        | 0.655 $\pm$ 0.020        | 0.001 $\pm$ 0.029        | 0.514 $\pm$ 0.016        | 0.440 $\pm$ 0.024        | 0.675 $\pm$ 0.012        | 0.079 $\pm$ 0.020        | 0.537 $\pm$ 0.008        |
|                             | unnormalized          | -0.114 $\pm$ 0.076       | 0.502 $\pm$ 0.029        | -0.107 $\pm$ 0.056       | 0.479 $\pm$ 0.026        | -0.105 $\pm$ 0.030       | 0.493 $\pm$ 0.020        | -0.079 $\pm$ 0.014       | 0.483 $\pm$ 0.010        |
| FV                          | normalized            | -0.065                   | 0.441                    | -0.398                   | 0.344                    | -0.051                   | 0.448                    | -0.369                   | 0.351                    |
|                             | unnormalized          | -0.528                   | 0.313                    | -0.411                   | 0.330                    | -0.514                   | 0.315                    | -0.388                   | 0.343                    |

as options for distance metric. In a similar manner, LL and FV are evaluated using both unnormalized  $h(\mathbf{x}) \in \mathbb{R}^d$  and normalized representations  $h(\mathbf{x})/\|h(\mathbf{x})\|_2 \in \mathcal{S}^{d-1}$ .

**Evaluation metric.** To evaluate our method and baselines, we employ two metrics: (i) the Pearson correlation coefficient (PCC) between the reliability and its estimate<sup>1</sup> and (ii) the area under the receiver operating characteristic curve (AUROC). For (ii), we call a data point’s representation reliable (positive) if the average accuracy is  $> 90\%$  (i.e., the average prediction error is  $\leq 0.1$ ).

## 4.2 Main Results

We evaluate the effectiveness of our proposed method (i.e., NC<sub>100</sub>) in capturing representation reliability. Table 1 indicates that neighborhood consistency NC<sub>100</sub> demonstrates a strong correlation with representation reliability compared with baselines. Additionally, our method is more robust with the choice of distance metric, while the baselines suffer from a significant performance reduction with different selections of the distance metric. Finally, FV shows no correlation with representation reliability, rendering it an inappropriate measure for evaluating representation reliability. This observation aligns with the theoretical results in Section 3.2.

### 4.2.1 Robustness to the Choice of Distance Metric

In order to examine the robustness of our method, we investigate the impact of different distance metrics. While Euclidean distance is a natural choice in  $\mathbb{R}^d$  where the representation lies, we also explore the applicability of cosine distance for our method and baselines. This is motivated by the fact that many recent self-supervised models, including SimCLR, are trained based on cosine similarity (i.e., the distance between the normalized vectors).

We observe that baseline methods, such as AvgDist<sub>k</sub> and LL, suffer from a significant performance reduction when paired with Euclidean distance. This reduction can even lead to a *negative* correlation with representation reliability. In contrast, our proposed method NC<sub>k</sub> consistently produces robust results regardless of the chosen distance metric. We further demonstrate these results with ResNet-18 in Figure 2 as well as Figure 5 in Appendix.

As observed in our results and Tack et al. (2020), points with a larger  $L_2$ -norm tend to exhibit higher reliability. This implies that reliable points are often located in the outer regions of the representation space, resulting in larger distances between points in those regions compared to points near the origin. Consequently, baseline metrics that rely on unnormalized feature vectors fail to capture reliability and may even show negative correlations, contrary to their speculations.

<sup>1</sup>The negative score is used for uncertainty measures, such as AvgDist<sub>k</sub> and FV.

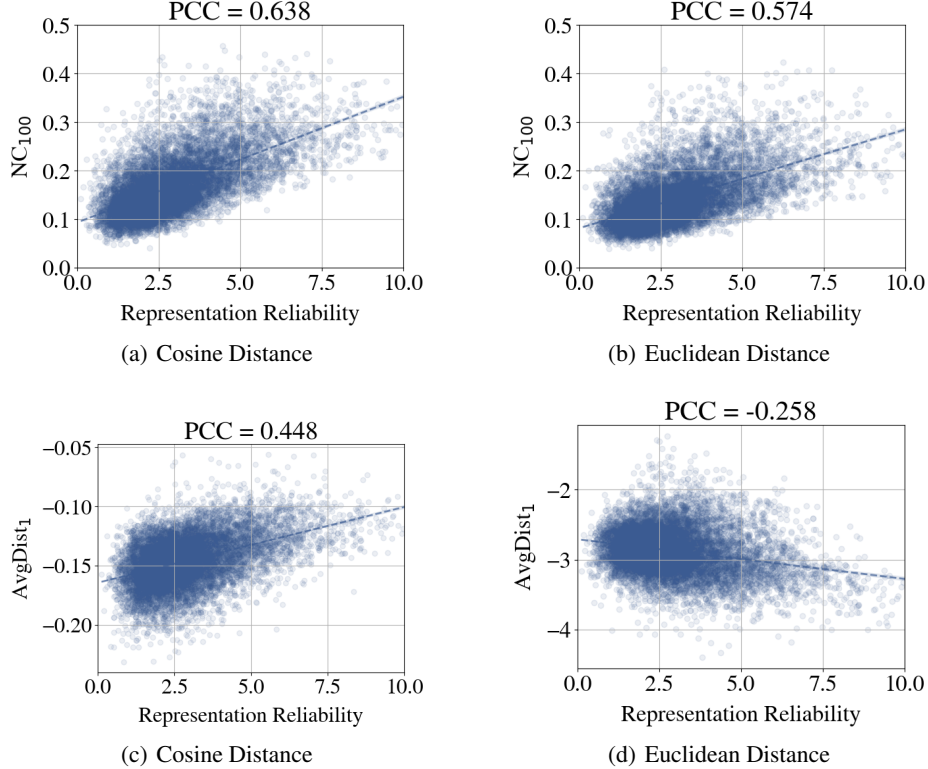


Figure 2: Scatter plots for comparing the representation reliability with the proposed method ( $NC_{100}$ ) and with baseline ( $AvgDist_1$ ), under different distance metrics on CIFAR-10. Ours exhibits a higher correlation with the representation reliability and is more robust to the choice of distance metric.

#### 4.2.2 Ablation Studies

**Trade-off on the number of neighbors ( $k$ ).** As discussed in Section 3.3, the choice of  $k$  in (8) leads to a trade-off between having more consistent neighbors and preserving the overall reliability of those neighbors. In order to explore this trade-off, we conduct experiments with different values of  $k \in \{1, 5, 10, 50, 100, 250, 500\}$ . The correlation between our proposed method and representation reliability is illustrated in Figure 3: it initially increases and then decreases as expected. We observe that the optimal performance is achieved with  $k$  between 50 and 100 for our method, while  $AvgDist_k$  performs well only with very small  $k$ .

**Effectiveness of the number of ensemble members ( $M$ ).** Figure 4 demonstrates that as the ensemble size increases, the evaluation metric becomes more robust and shows improved performance. Furthermore, even with just  $M = 2$  ensemble members, our approach significantly outperforms other baselines. Overall, these results align with the trends presented by Lakshminarayanan et al. (2017), and highlight how neighborhood consistency effectively extends the deep ensemble approach from supervised learning to unsupervised representation learning.

## 5 Final Remarks and Limitations

Self-supervised learning is increasingly used for training general-purpose embedding functions that can be adapted to various downstream tasks. In this paper, we present a systematic study to evaluate the quality of representations assigned by the embedding functions. We introduce a mathematical definition of representation reliability, demonstrate that existing uncertainty frameworks in supervised learning do not capture representation reliability, derive an estimate for representation reliability, and validate our estimate through extensive numerical experiments.



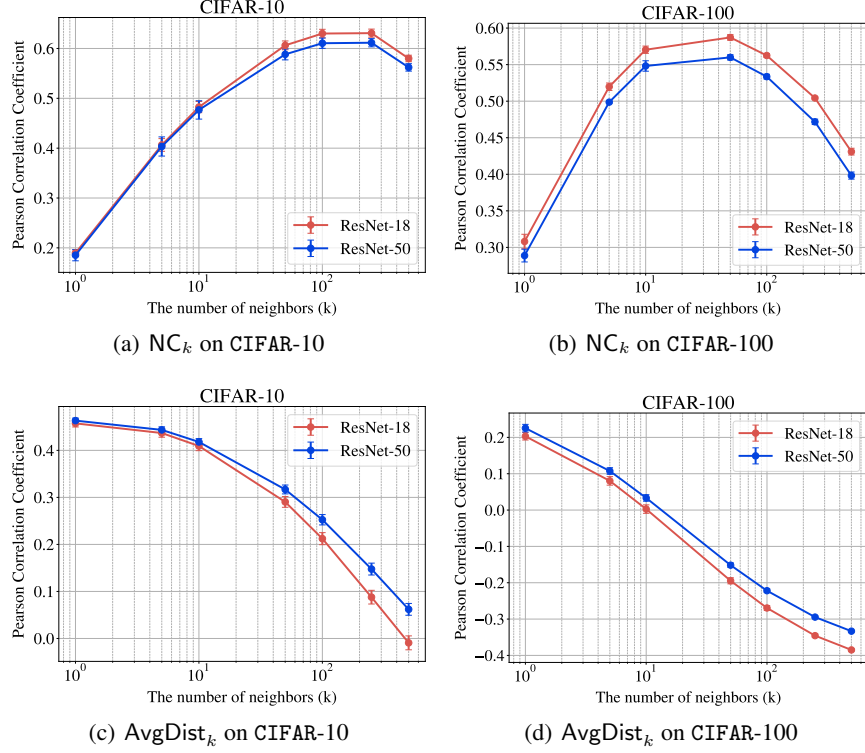


Figure 3: Ablation over the number of neighboring points ( $k$ ) for the proposed method ( $NC_k$ ) and the baseline ( $AvgDist_k$ ). The figures report models using cosine distance.

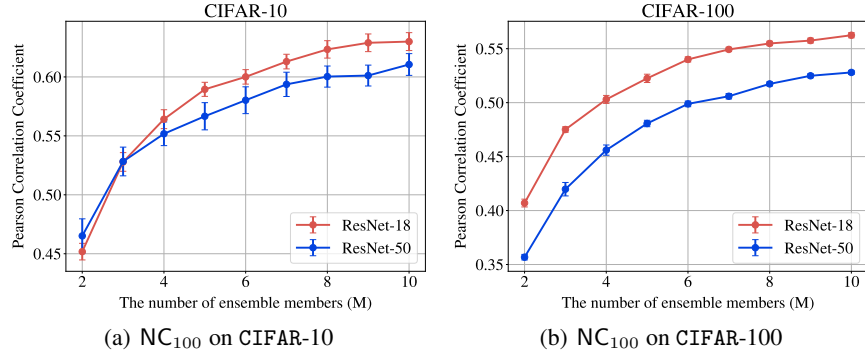


Figure 4: Ablation over the number of ensemble functions ( $M$ ). The performance of our proposed method improves as  $M$  increases. The figures report models using cosine distance.

There is a crucial need for future research to investigate and ensure the responsibility and trustworthiness of embedding functions. For example, representations should be interpretable and not compromise private information. Moreover, the embedding functions should exhibit robustness against adversarial attacks and incorporate a notion of uncertainty, in addition to their abstract representations. This work takes an initial step towards understanding the uncertainty of the representations. In the case where a downstream model fails to deliver a desirable output for a test point, the representation reliability can provide valuable insight into whether the mistake was due to unreliable representations or downstream heads.

There are several potential future directions that are worth further exploration. For example, our current method for estimating representation reliability uses a set of embedding functions to compute neighborhood consistency. It would be interesting to investigate whether our approach can be

expanded to avoid the need for training multiple embedding functions. This could potentially be achieved through techniques such as MC dropout or adding random noise to the neural network parameters in order to perturb them slightly. Additionally, while we currently assess representation reliability through downstream prediction tasks, it would be valuable to investigate the generalization of our definition to encompass a broader range of downstream tasks.

## References

- Achille, A. and Soatto, S. (2017). On the emergence of invariance and disentangling in deep representations. *arXiv preprint arXiv:1706.01350*, 125:126–127.
- Al-Tahan, H. and Mohsenzadeh, Y. (2021). Clar: Contrastive learning of auditory representations. In *International Conference on Artificial Intelligence and Statistics*, pages 2530–2538. PMLR.
- Alemi, A. A., Fischer, I., Dillon, J. V., and Murphy, K. (2016). Deep variational information bottleneck. *arXiv preprint arXiv:1612.00410*.
- Ardeshtir, S. and Azizan, N. (2022). Uncertainty in contrastive learning: On the predictability of downstream performance. *arXiv preprint arXiv:2207.09336*.
- Bojchevski, A. and Günnemann, S. (2017). Deep Gaussian embedding of graphs: Unsupervised inductive learning via ranking. *arXiv preprint arXiv:1707.03815*.
- Bommasani, R., Hudson, D. A., Adeli, E., Altman, R., Arora, S., von Arx, S., Bernstein, M. S., Bohg, J., Bosselut, A., Brunskill, E., et al. (2021). On the opportunities and risks of foundation models. *arXiv preprint arXiv:2108.07258*.
- Brown, T., Mann, B., Ryder, N., Subbiah, M., Kaplan, J. D., Dhariwal, P., Neelakantan, A., Shyam, P., Sastry, G., Askell, A., et al. (2020). Language models are few-shot learners. *Advances in neural information processing systems*, 33:1877–1901.
- Chen, T., Kornblith, S., Norouzi, M., and Hinton, G. (2020a). A simple framework for contrastive learning of visual representations. In *International conference on machine learning*, pages 1597–1607. PMLR.
- Chen, X., Fan, H., Girshick, R., and He, K. (2020b). Improved baselines with momentum contrastive learning. *arXiv preprint arXiv:2003.04297*.
- Daxberger, E., Kristiadi, A., Immer, A., Eschenhagen, R., Bauer, M., and Hennig, P. (2021). Laplace redux-effortless Bayesian deep learning. *Advances in Neural Information Processing Systems*, 34:20089–20103.
- Depeweg, S., Hernandez-Lobato, J.-M., Doshi-Velez, F., and Udluft, S. (2018). Decomposition of uncertainty in Bayesian deep learning for efficient and risk-sensitive learning. In *International Conference on Machine Learning*, pages 1184–1193. PMLR.
- Gal, Y. and Ghahramani, Z. (2016). Dropout as a Bayesian approximation: Representing model uncertainty in deep learning. In *international conference on machine learning*, pages 1050–1059. PMLR.
- Hadsell, R., Chopra, S., and LeCun, Y. (2006). Dimensionality reduction by learning an invariant mapping. In *2006 IEEE Computer Society Conference on Computer Vision and Pattern Recognition (CVPR’06)*, volume 2, pages 1735–1742. IEEE.
- He, K., Fan, H., Wu, Y., Xie, S., and Girshick, R. (2020). Momentum contrast for unsupervised visual representation learning. In *Proceedings of the IEEE/CVF conference on computer vision and pattern recognition*, pages 9729–9738.
- He, K., Zhang, X., Ren, S., and Sun, J. (2016). Deep residual learning for image recognition. In *Proceedings of the IEEE conference on computer vision and pattern recognition*, pages 770–778.
- Jaiswal, A., Babu, A. R., Zadeh, M. Z., Banerjee, D., and Makedon, F. (2020). A survey on contrastive self-supervised learning. *Technologies*, 9(1):2.

- Jing, L. and Tian, Y. (2020). Self-supervised visual feature learning with deep neural networks: A survey. *IEEE transactions on pattern analysis and machine intelligence*, 43(11):4037–4058.
- Karaletsos, T., Belongie, S., and Rätsch, G. (2015). Bayesian representation learning with oracle constraints. *arXiv preprint arXiv:1506.05011*.
- Kendall, A. and Gal, Y. (2017). What uncertainties do we need in Bayesian deep learning for computer vision? *Advances in neural information processing systems*, 30.
- Krizhevsky, A., Hinton, G., et al. (2009). Learning multiple layers of features from tiny images.
- Lakshminarayanan, B., Pritzel, A., and Blundell, C. (2017). Simple and scalable predictive uncertainty estimation using deep ensembles. *Advances in neural information processing systems*, 30.
- Lee, K., Lee, K., Lee, H., and Shin, J. (2018). A simple unified framework for detecting out-of-distribution samples and adversarial attacks. *Advances in neural information processing systems*, 31.
- MacKay, D. J. (1992). A practical Bayesian framework for backpropagation networks. *Neural computation*, 4(3):448–472.
- Mirzae, H., Salehi, M., Shahabi, S., Gavves, E., Snoek, C. G., Sabokrou, M., and Rohban, M. H. (2022). Fake it till you make it: Towards accurate near-distribution novelty detection.
- Morgado, P., Vasconcelos, N., and Misra, I. (2021). Audio-visual instance discrimination with cross-modal agreement. In *Proceedings of the IEEE/CVF Conference on Computer Vision and Pattern Recognition*, pages 12475–12486.
- Neal, R. M. (1996). *Bayesian learning for neural networks*. Springer-Verlag, Berlin, Heidelberg.
- Neelakantan, A., Shankar, J., Passos, A., and McCallum, A. (2015). Efficient non-parametric estimation of multiple embeddings per word in vector space. *arXiv preprint arXiv:1504.06654*.
- Oh, S. J., Murphy, K., Pan, J., Roth, J., Schroff, F., and Gallagher, A. (2018). Modeling uncertainty with hedged instance embedding. *arXiv preprint arXiv:1810.00319*.
- OpenAI (2022). Chatgpt: Optimizing language models for dialogue. <https://openai.com/blog/chatgpt/>.
- Osband, I., Aslanides, J., and Cassirer, A. (2018). Randomized prior functions for deep reinforcement learning. *Advances in Neural Information Processing Systems*, 31.
- Radford, A., Kim, J. W., Hallacy, C., Ramesh, A., Goh, G., Agarwal, S., Sastry, G., Askell, A., Mishkin, P., Clark, J., et al. (2021). Learning transferable visual models from natural language supervision. In *International Conference on Machine Learning*, pages 8748–8763. PMLR.
- Sharma, A., Azizan, N., and Pavone, M. (2021). Sketching curvature for efficient out-of-distribution detection for deep neural networks. In *Uncertainty in Artificial Intelligence*, pages 1958–1967. PMLR.
- Tack, J., Mo, S., Jeong, J., and Shin, J. (2020). CSI: Novelty detection via contrastive learning on distributionally shifted instances. *Advances in neural information processing systems*, 33:11839–11852.
- Tran, D., Liu, J., Dusenberry, M. W., Phan, D., Collier, M., Ren, J., Han, K., Wang, Z., Mariet, Z., Hu, H., et al. (2022). Plex: Towards reliability using pretrained large model extensions. *arXiv preprint arXiv:2207.07411*.
- van Amersfoort, J., Smith, L., Teh, Y. W., and Gal, Y. (2020). Uncertainty estimation using a single deep deterministic neural network. In *International conference on machine learning*, pages 9690–9700. PMLR.
- Vilnis, L. and McCallum, A. (2015). Word representations via Gaussian embedding. In Bengio, Y. and LeCun, Y., editors, *3rd International Conference on Learning Representations, ICLR 2015, San Diego, CA, USA, May 7-9, 2015, Conference Track Proceedings*.

- Wen, Y., Tran, D., and Ba, J. (2020). Batchensemble: an alternative approach to efficient ensemble and lifelong learning. *arXiv preprint arXiv:2002.06715*.
- Wu, M. and Goodman, N. (2020). A simple framework for uncertainty in contrastive learning. *arXiv preprint arXiv:2010.02038*.
- Zhang, O., Wu, M., Bayrooti, J., and Goodman, N. (2021). Temperature as uncertainty in contrastive learning. In *NeurIPS Workshop on Self-Supervised Learning*.

## A Theoretical Results and Omitted Proofs

### A.1 Proof of Theorem 1

*Proof.* Recall that downstream task  $t$  is a regression problem that applies the empirical risk minimization to a dataset  $\{(\mathbf{x}_{t,i}, y_{t,i})\}_{i \in [n_t]}$  to find an optimal linear head. We denote  $\mathbf{y}_t = (y_{t,1}, \dots, y_{t,n_t})^T$  and assume that there are only two embedding functions without loss of generality. We choose  $h_1(\mathbf{x}) = -h_2(\mathbf{x})$  and let  $\|h_1(\mathbf{x})\|_2^2 \geq A$  for any  $\mathbf{x}$ .

We construct a matrix  $\mathbf{H}_{k,t} \in \mathbb{R}^{n_t \times d}$  such that each row of  $\mathbf{H}_{k,t}$  is  $h_k(\mathbf{x}_{t,i})$ . By our construction,  $\mathbf{H}_{1,t} = -\mathbf{H}_{2,t}$ . Since we apply the empirical risk minimization, the optimal linear head  $g_{k,t}(\mathbf{z}) = \mathbf{w}_{k,t}^T \mathbf{z}$  satisfies

$$\mathbf{w}_{k,t} = (\mathbf{H}_{k,t}^T \mathbf{H}_{k,t})^{-1} \mathbf{H}_{k,t}^T \mathbf{y}_t \quad (9)$$

assuming  $\mathbf{H}_{k,t}^T \mathbf{H}_{k,t}$  is invertible. Therefore, we have  $\mathbf{w}_{1,t} = -\mathbf{w}_{2,t}$ . As a result, for a new test point  $\mathbf{x}^*$ , although  $h_1(\mathbf{x}^*) = -h_2(\mathbf{x}^*)$ , their prediction outcome is the same  $g_{1,t} \circ h_1(\mathbf{x}^*) = g_{2,t} \circ h_2(\mathbf{x}^*)$ , which leads to the desired conclusion:

$$\text{Var}_{k \sim [K]}(h_k(\mathbf{x}^*)) \geq A \quad \text{and} \quad \text{Var}_{k \sim [K]}(g_{k,t} \circ h_k(\mathbf{x}^*)) = 0. \quad (10)$$

□

### A.2 Linking Representation Distance to Output Difference

**Lemma 1.** *For a given test point  $\mathbf{x}^*$ , suppose there exists a neighbor  $\mathbf{x}$  in the representation space, constructed by the embedding function  $h$ :*

$$\|h(\mathbf{x}) - h(\mathbf{x}^*)\|_2 \leq \epsilon_{nb}. \quad (11)$$

*For a downstream predictor  $g(\mathbf{z}) = a(\mathbf{w}^T \mathbf{z} + b)$ , the prediction at  $\mathbf{x}^*$  is similar to the prediction at  $\mathbf{x}$ :*

$$|g \circ h(\mathbf{x}) - g \circ h(\mathbf{x}^*)| \leq \|\mathbf{w}\|_2 \cdot \epsilon_{nb}. \quad (12)$$

*Proof.* Suppose  $a(\cdot)$  is 1-Lipschitz continuous (e.g., sigmoid and identity),

$$\begin{aligned} |g \circ h(\mathbf{x}) - g \circ h(\mathbf{x}^*)| &= |g \circ h(\mathbf{x}) - g \circ h(\mathbf{x}^*)| \\ &= |a(\mathbf{w}^T h(\mathbf{x}) + b) - a(\mathbf{w}^T h(\mathbf{x}^*) + b)| \\ &\leq 1 \cdot |(\mathbf{w}^T h(\mathbf{x}) + b) - (\mathbf{w}^T h(\mathbf{x}^*) + b)| \\ &= |\mathbf{w}^T (h(\mathbf{x}) - h(\mathbf{x}^*))| \\ &\leq \|\mathbf{w}\|_2 \cdot \|h(\mathbf{x}) - h(\mathbf{x}^*)\|_2 \\ &\leq \|\mathbf{w}\|_2 \cdot \epsilon_{nb}. \end{aligned} \quad (13)$$

□

### A.3 Proof of Theorem 2

*Proof.* First, we denote  $f_i = g_{i,t} \circ h_i$ . By Lemma 1, we have

$$|f_i(\mathbf{x}^r) - f_i(\mathbf{x}^*)| \leq \|\mathbf{w}_{i,t}\|_2 \cdot \epsilon_{nb} = \epsilon_{nb}. \quad (14)$$

By the triangle inequality, we have the following upper bound for the output difference:

$$\begin{aligned} |f_i(\mathbf{x}^*) - f_j(\mathbf{x}^*)| &\leq |f_i(\mathbf{x}^*) - f_i(\mathbf{x}^r)| + |f_i(\mathbf{x}^r) - y^r| + |y^r - f_j(\mathbf{x}^r)| + |f_j(\mathbf{x}^r) - f_j(\mathbf{x}^*)| \\ &\leq (\epsilon_{nb} + \epsilon_r + \epsilon_r + \epsilon_{nb}) \\ &= 2(\epsilon_{nb} + \epsilon_r). \end{aligned} \quad (15)$$

Since the ensemble variance is equivalent to the average pairwise difference across the ensemble of  $f_i$ , thus bounded by:

$$\begin{aligned}\text{Var}_{i \sim [M]}(g_{i,t} \circ h_i(\mathbf{x}^*)) &= \frac{1}{M^2} \sum_{i < j} |f_i(\mathbf{x}^*) - f_j(\mathbf{x}^*)|^2 \\ &\leq \frac{1}{M^2} \sum_{i < j} 4(\epsilon_{nb} + \epsilon_r)^2 = \frac{M(M-1)}{2M^2} 4(\epsilon_{nb} + \epsilon_r)^2 \\ &= 2 \left(1 - \frac{1}{M}\right) (\epsilon_{nb} + \epsilon_r)^2.\end{aligned}\tag{16}$$

□

## B Connection between NC and Downstream Uncertainty

### B.1 Posterior Predictive Distribution in Downstream tasks

Consider a class of embedding functions  $\mathcal{H}$ , where each function (i.e., representation model)  $h$  generates a representation vector  $p(\mathbf{z} \mid \mathbf{x}, h)$  for an input variable  $\mathbf{x}$ . For downstream task  $t$ , this paper focuses on the case where downstream predictor  $g_t$  is built upon the fixed representation space  $\mathcal{Z}_h$  constructed by the embedding function  $h$ . Denote a pre-training dataset and a downstream training dataset as  $\mathcal{D}_t$  and  $\mathcal{D}_p$ , respectively. Also, denote the whole dataset as  $\mathcal{D} = \mathcal{D}_p \cup \mathcal{D}_t$ . Following the Bayesian framework described in Section 2, the joint posterior distribution on the embedding function and predictor is given by:

$$\begin{aligned}p(g, h \mid \mathcal{D}) &= p(g \mid h, \mathcal{D}_t, \mathcal{D}_p) p(h \mid \mathcal{D}_t, \mathcal{D}_p) \\ &= p(g \mid h, \mathcal{D}) p(h \mid \mathcal{D}_p).\end{aligned}\tag{17}$$

Assuming that the downstream task is relatively simple to the extent that the uncertainty over the downstream predictor is negligible, the posterior distribution over  $\mathcal{D}_t$  can be considered highly sharp around the optimal predictor  $g_t$ <sup>2</sup>:

$$p(g \mid h, \mathcal{D}_t) \approx \delta(g - g_t).\tag{18}$$

For a new test point  $\mathbf{x}^*$ , its posterior predictive distribution is obtained by averaging the predictive probabilities over models:

$$\begin{aligned}p(\hat{y}^* \mid \mathbf{x}^*, \mathcal{D}) &= \int p(\hat{y}^* \mid \mathbf{x}^*, g, h) p(g, h \mid \mathcal{D}) d\mathbf{f} \\ &= \int p(\hat{y}^* \mid \mathbf{z}^*, g) p(\mathbf{z}^* \mid \mathbf{x}^*, h) p(g \mid h, \mathcal{D}_t) p(h \mid \mathcal{D}_p) dg dh \\ &= \mathbb{E}_{h \sim p(\cdot \mid \mathcal{D}_p)} [p(\hat{y}^* \mid \mathbf{z}^*, g_t) p(\mathbf{z}^* \mid \mathbf{x}^*, h)].\end{aligned}\tag{19}$$

We can further approximate the posterior predictive with Monte Carlo approach:

$$p(\hat{y}^* \mid \mathbf{x}^*, \mathcal{D}) \approx \frac{1}{M} \sum_{i=1}^M [\delta(\hat{y}^* - g_t \circ h_i(\mathbf{x}^*))].\tag{20}$$

In summary, we can approximate the posterior predictive by: 1) training multiple embedding functions, 2) training optimal downstream predictors upon each representation model, and 3) taking the empirical distribution of outputs as the posterior. Using a Bayesian downstream predictor (instead of a single point estimator) or sampling multiple downstream predictors is a simple way to further improve the approximation.

---

<sup>2</sup>In simpler terms, the prior distribution over the predictors is considered to be the class of optimal solutions generated by the learning algorithm  $\mathcal{A}_t$  under the embedding function  $h$ .



## B.2 Monte Carlo Approximation of the Downstream Uncertainty

First of all, recall the ensemble variance appeared in Equation 7 of Theorem 2. It represents the predictive variance for the downstream task  $t$  when considering the ensemble of embedding functions  $h_1, \dots, h_M$ . Furthermore, as discussed in Appendix B.1, each composition  $g_{t,i} \circ h_i$  can be seen as a function sampled from the posterior distribution  $p(\cdot \mid \mathcal{D}_p, \mathcal{D}_t)$ .

Hence, the ensemble variance serves as an approximation of the variance across the posterior predictive distribution, similar to the approach taken in the Monte Carlo method discussed in Section 2:

$$\text{Var}_{i \sim [M]} (g_{t,i} \circ h_i(\mathbf{x}^*)) \approx \text{Var}(\hat{y}^* \mid \mathbf{x}^*, \mathcal{D}_p, \mathcal{D}_t). \quad (21)$$

While establishing a rigorous relationship between uncertainty and predictive accuracy may pose challenges, empirical studies have demonstrated a strong correlation between the two measures; we also observe that data points with high predictive variance tend to exhibit lower average accuracy. This follows from the intuition that a higher level of uncertainty in the prediction indicates that the predictor is less certain of its guess, which is likely to be incorrect.

## C More Details on Neighborhood Consistency

### C.1 Representation Alignment

In this section, we present an alternative viewpoint to clarify the underlying motivation behind neighborhood consistency and demonstrate how it addresses the shortcomings of existing supervised learning frameworks. As illustrated in Section 2, the uncertainty in supervised learning could be expressed by the variance of predictions across various functions. It is important to note that this approach is applicable since different functions transform the input into the "same" output space and the distance/similarity within the output space is well-defined.

From the perspective of unsupervised learning, however, there is no "unique" ground truth representation space which makes it difficult to compare the representations constructed by different embedding functions. Therefore, to properly measure the distance between the pair of representation vectors  $p$  and  $q$ , we need a transformation function  $\phi(\cdot)$  that maps different representations into a comparable form. Then, the consistency across the set of representations  $\{h_1(\mathbf{x}), \dots, h_M(\mathbf{x})\}$  can be assessed as follows:

$$\text{ReprConsistency}(\mathbf{x}) = \frac{1}{M^2} \sum_{i < j} \text{Sim}(\phi(\mathbf{z}_i), \phi(\mathbf{z}_j)) \quad (22)$$

where  $\phi(\mathbf{z}_i)$  can be viewed as a *surrogate representation* of  $\mathbf{z}_i = h_i(\mathbf{x})$ .

What characteristics should an appropriate  $\phi(\cdot)$  have? First and foremost, it would require an anchor that connects different representation spaces, and this paper suggests using (reliable) "pre-training data" as such anchors. As such, we first introduce a surrogate vector representation consisting of the relative distances from the test point to each reference point:

$$\phi_{\text{rel-fc}}(\mathbf{z}_i^*; \mathbf{Z}_{i,\text{ref}}) \triangleq \left[ \text{dist}(\mathbf{z}_i^*, \mathbf{z}_i^{(1)}), \dots, \text{dist}(\mathbf{z}_i^*, \mathbf{z}_i^{(n)}) \right]^T \quad (23)$$

where  $\mathbf{Z}_{i,\text{ref}} = \{\mathbf{z}_i^{(l)} = h_i(\mathbf{x}^{(l)})\}_{l=1}^n$  is a set of representation vectors of (reliable) reference data, and  $\text{dist}(\cdot)$  is a distance metric in the representation space, upon the embedding function  $h_i(\cdot)$ . The proposed representation captures the relational information among neighboring data points, placing less emphasis on the absolute location of the representation features for new data.

The aforementioned representation, however, is burdened with an excessive amount of information; it also takes into account the distant neighbors, complicating the representation, thereby posing a risk to its overall performance in practice. To address the issue, we propose a *sparsified representation* as follows:

$$\phi_{\text{rel-sparse}}(\mathbf{z}_i^*; \mathbf{Z}_{i,\text{ref}}) \triangleq \left[ \mathbb{1}(\text{dist}(\mathbf{z}_i^*, \mathbf{z}_i^{(1)}) \leq \epsilon), \dots, \mathbb{1}(\text{dist}(\mathbf{z}_i^*, \mathbf{z}_i^{(n)}) \leq \epsilon) \right]^T \quad (24)$$

where  $\mathbb{1}$  is an indicator function; and  $\epsilon \in \mathbb{R}$  is a small real number. The equivalent set notation of the vector representation is:  $\epsilon\text{-NN}_i(\mathbf{x}^*) \triangleq \{l \mid \text{dist}(h_i(\mathbf{x}^*), h_i(\mathbf{x}^{(l)})) \leq \epsilon\}$ . The corresponding

| Surrogate Representations  | Graph           | Representation | Sim              |
|----------------------------|-----------------|----------------|------------------|
| $\phi_{\text{rel-fc}}$     | Fully-Connected | Vector         | L1, L2 distance  |
| $\phi_{\text{rel-sparse}}$ | Sparse          | Vector         | L1, L2 distance  |
| $\epsilon\text{-NN}$       | Sparse          | Set            | Jaccard, Overlap |
| $k\text{-NN}$              | Sparse          | Set            | Jaccard, Overlap |

Table 2: Graph-based representations for measuring representation consistency.

neighborhood consistency measure can be computed as follows:

$$\text{NC}_\epsilon(\mathbf{x}^*) \triangleq \frac{1}{M^2} \sum_{i < j} \text{Sim}(\epsilon\text{-NN}_i(\mathbf{x}^*), \epsilon\text{-NN}_j(\mathbf{x}^*)). \quad (25)$$

However, selecting an appropriate value for  $\epsilon$  can be challenging since determining the proper scale of the representation space is not straightforward. As a result, we introduce a scale-free version of neighborhood consistency that relies on the local  $k$ -nearest neighborhood:

$$\text{NC}_k(\mathbf{x}^*) \triangleq \frac{1}{M^2} \sum_{i < j} \text{Sim}(k\text{-NN}_i(\mathbf{x}^*), k\text{-NN}_j(\mathbf{x}^*)) \quad (26)$$

where  $k\text{-NN}_i(\mathbf{x}^*)$  is the index set of  $k$  nearest neighbors of  $h_i(\mathbf{x}^*)$  among  $\mathbf{Z}_{i,\text{ref}}$ .

For a set similarity metric  $\text{Sim}$ , we can use either *Jaccard Similarity* or *Overlap Coefficient*:

$$\text{Jaccard Similarity}(S_1, S_2) \triangleq \frac{|S_1 \cap S_2|}{|S_1 \cup S_2|} \quad (27)$$

$$\text{Overlap Coefficient}(S_1, S_2) \triangleq \frac{|S_1 \cap S_2|}{\min(|S_1|, |S_2|)}. \quad (28)$$

If the size of  $S_1$  and  $S_2$  are equal to  $k$ :  $|S_1 \cup S_2| = 2k - |S_1 \cap S_2|$  and  $\min(|S_1|, |S_2|) = k$ . Thus, regardless of the selection, both similarity metrics solely depends on  $|S_1 \cap S_2|$  when the  $k\text{-NN}$  approach is used to determine the neighbors. Additionally, given a set of test points, both metrics provide the same order (i.e., rank) in terms of their representation reliability; thus show the same AUROC performance.

## C.2 Graph-Representation View of Neighborhood Consistency

The surrogate representation introduced in Section C.1 can be viewed as a *graph representation* that is characterized by a (weighted) graph that captures the relative relationships among data points.

In particular, suppose a test point lies within reference points. In this case,  $\phi_{\text{rel-fc}}$  represents an adjacency vector of a fully connected weighted graph. More specifically, the set of nodes in this graph is  $\mathcal{V}_i \triangleq \mathbf{Z}_{i,\text{ref}}$  while the edge weight between two nodes is determined by  $\text{dist}(\cdot, \cdot)$ .

Additionally,  $\phi_{\text{rel-sparse}}$  represents an adjacency vector of an unweighted sparsified graph  $(\mathcal{V}_i, \mathcal{E}_i)$ . Here,  $\mathcal{E}_i$  is defined as  $\{(m, l) \mid \text{dist}(h_i(\mathbf{x}^{(m)}), h_i(\mathbf{x}^{(l)})) \leq \epsilon\}$ . This means that two nodes are connected in the sparsified graph if the distance between the corresponding data points, as determined by  $\text{dist}(\cdot, \cdot)$ , is less than or equal to  $\epsilon$ .

Finally,  $\epsilon\text{-NN}_i$  and  $k\text{-NN}_i$  refer to the sets of adjacent nodes in each sparsified graph.

Table 2 provides a summary of the surrogate representation examples mentioned above, along with the recommended choices for the corresponding  $\text{Sim}$  metric.

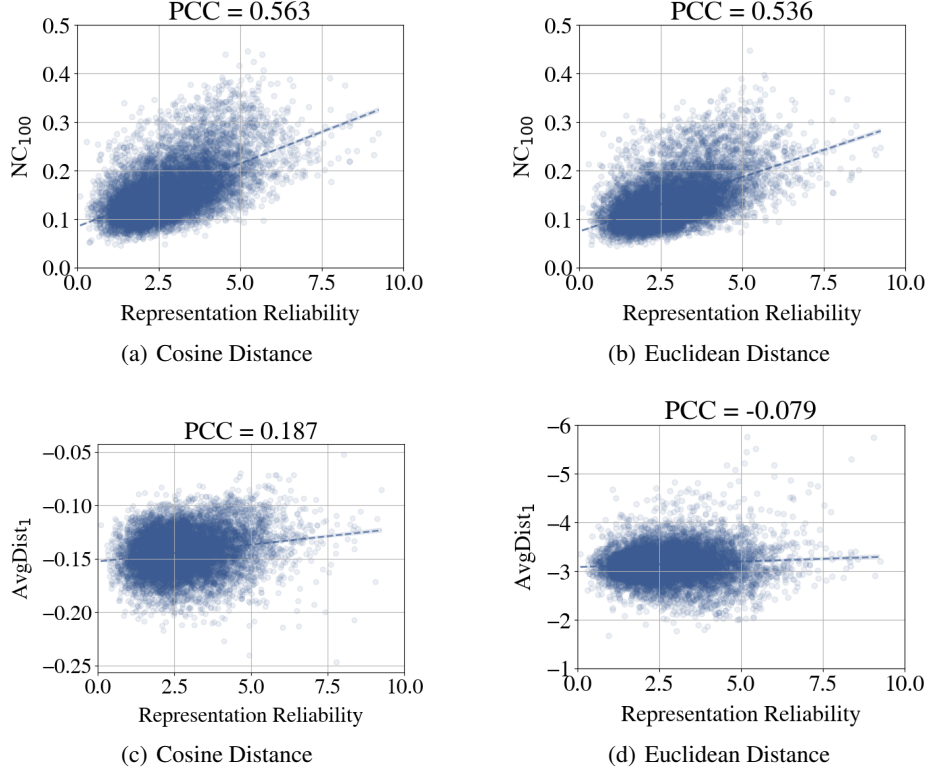


Figure 5: Scatter plots for comparing the representation reliability with the proposed method ( $NC_{100}$ ) and with baseline ( $AvgDist_1$ ), under different distance metrics on CIFAR-100 with ResNet-18. Ours exhibits a higher correlation with the representation reliability and is more robust to the choice of distance metric.

## D Additional Experimental Results

**Robustness to the Choice of Distance Metric.** We observe that baseline methods suffer from a significant performance reduction when paired with Euclidean distance. In contrast, our proposed method  $NC_k$  consistently produces robust results regardless of the chosen distance metric. We demonstrate these results in: Figure 2 (CIFAR-10 with ResNet-18), Figure 5 (CIFAR-100 with ResNet-18) as well as Figure 6 (CIFAR-10 with ResNet-50), and Figure 7 (CIFAR-100 with ResNet-50).

**Ablation over  $\phi$  and Sim metric.** We employ the  $\epsilon$ -NN approach to carry out an ablation study over  $\phi$ . We empirically observe that for both approaches, cosine distance performs better than Euclidean distance. In addition, we tested  $\epsilon = \{0.2, 0.25, 0.3, 0.35, 0.4\}$  and  $\epsilon = 0.25$  shows the best performance.

Then, we compare  $\epsilon$ -NN with  $\epsilon = 0.25$  to  $k$ -NN with  $k = 100$ . The experimental result is illustrated in Figure 8. First of all, as shown in the figure, the  $k$ -NN approach demonstrates a stronger correlation to the  $\epsilon$ -NN approach. Additionally, when using the  $k$ -NN approach, the choice of Sim metric does not have a significant impact on performance.

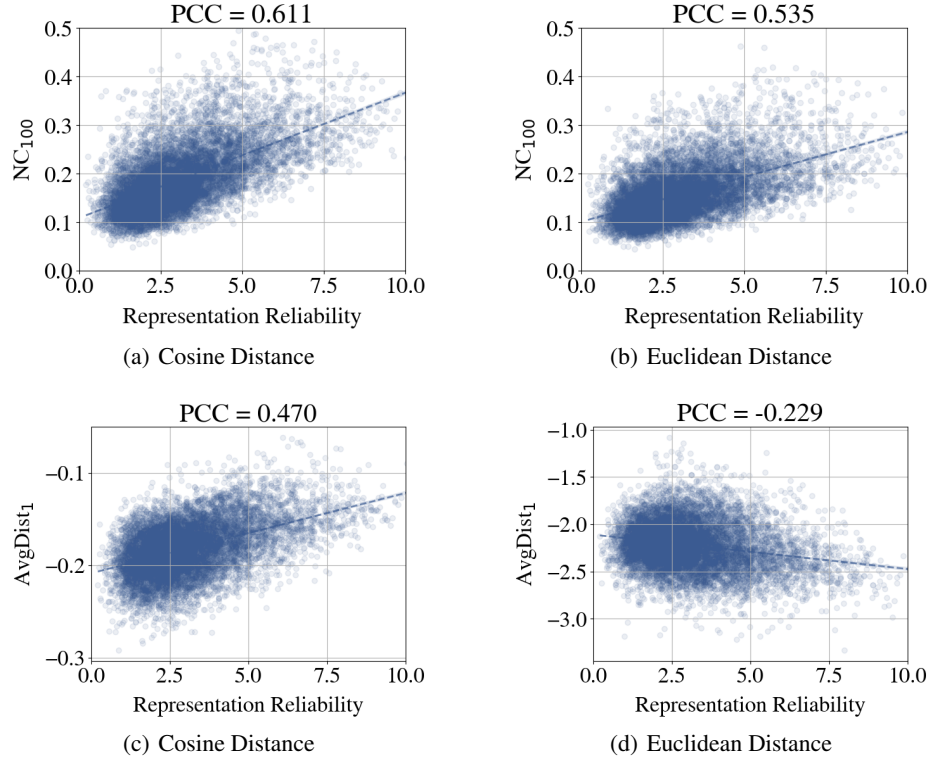


Figure 6: Scatter plots for comparing the representation reliability with the proposed method ( $NC_{100}$ ) and with baseline ( $AvgDist_1$ ), under different distance metrics on CIFAR-10 with ResNet-50. Ours exhibits a higher correlation with the representation reliability and is more robust to the choice of distance metric.

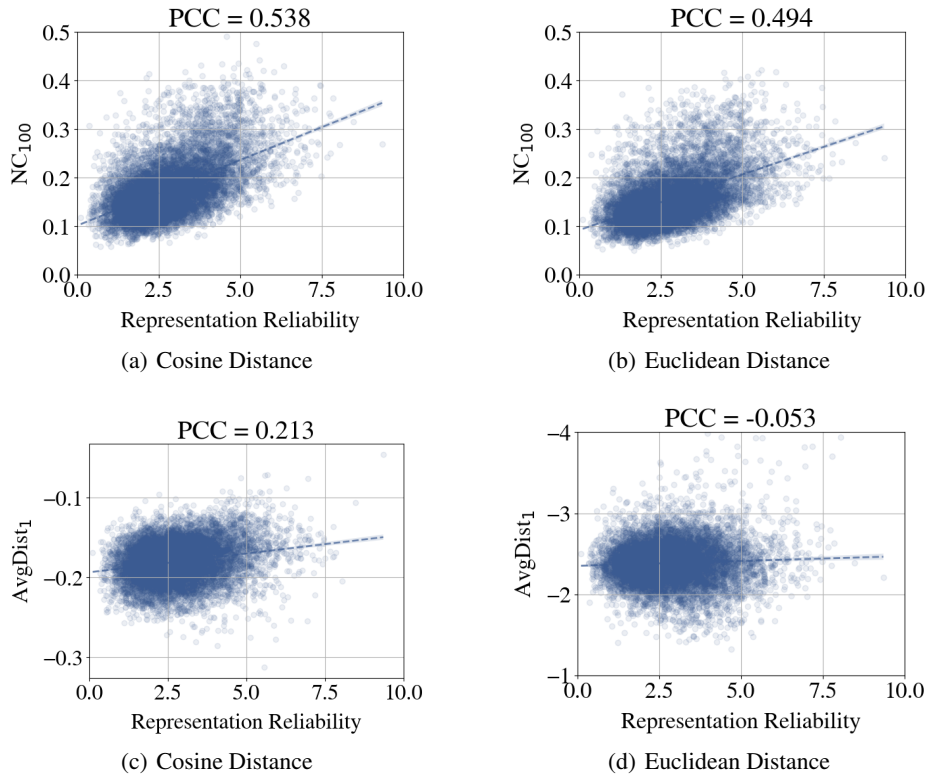


Figure 7: Scatter plots for comparing the representation reliability with the proposed method ( $NC_{100}$ ) and with baseline ( $AvgDist_1$ ), under different distance metrics on CIFAR-100 with ResNet-50. Ours exhibits a higher correlation with the representation reliability and is more robust to the choice of distance metric.

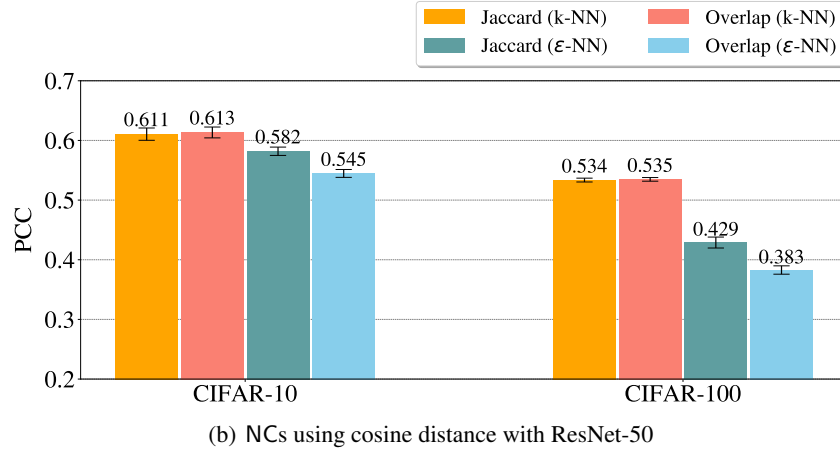
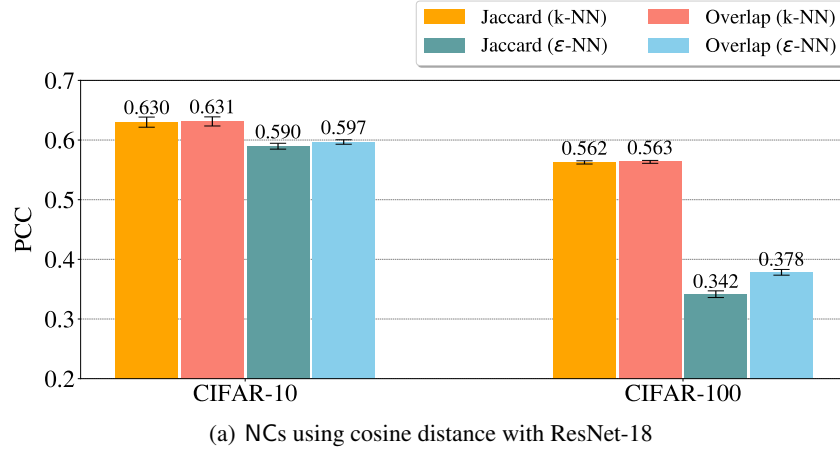


Figure 8: Bar plots for comparing  $NC_k$  with  $k = 100$  and  $NC_\epsilon$  with  $\epsilon = 0.25$ , under cosine distance on CIFAR-10 and CIFAR-100. Overall, the  $k$ -NN approach demonstrates a higher Pearson correlation coefficient (PCC) to the  $\epsilon$ -NN approach. Furthermore, the selection of Sim metric barely affect the performance of  $k$ -NN approach.



## E More on Related Work

Self-Supervised representation learning has become standard in many computer vision applications. Instead of training a neural network that takes in the raw data and outputs the target value (e.g., class label), it optimizes a neural network  $h_\theta$  that maps an input  $x$  into the latent vector  $z \in \mathbb{R}^d$  in the  $d$ -dimensional representation space.

Uncertainty estimation is the process of figuring out how uncertain or reliable the learned representations of the data are. Assessing the uncertainty of the neural network’s representation is a key step in making a reliable machine learning framework. This is because the uncertainty provides information about the data and how confident the model is in its modeling. There are several ways to estimate uncertainty in deep learning, such as Bayesian approaches and ensembling, in supervised learning settings where the ground truth output (e.g., label) is given. Estimating uncertainty in deep representation learning, on the other hand, is still a relatively undiscovered area of research.

### E.1 Uncertainty-aware Representation Learning

The representation model is often considered to be deterministic in recently popular frameworks (Chen et al., 2020a; He et al., 2020; Chen et al., 2020b). To address the reliability issue of those frameworks, some recent works, including (Oh et al., 2018; Wu and Goodman, 2020), extend the prior deterministic frameworks to stochastic ones, allowing for the construction of an uncertainty-aware self-Supervised representation learning framework.

Oh et al. (2018) introduces a hedged instance embedding (HIB) that optimizes a representation network that approximates the distribution over the representation vector  $p_\theta(z|x)$  under the (soft) contrastive loss (Hadsell et al., 2006) and variational information bottleneck (VIB) principle (Alemi et al., 2016; Achille and Soatto, 2017). More specifically, HIB encoder parameterizes the distribution as the mixture of  $C$  Gaussians:  $p_\theta(z|x) = \sum_{c=1}^C \mathcal{N}(z; \mu_\theta(x, c), \Sigma_\theta(x, c))$ . Based on the stochastic embedding, the paper proposes an uncertainty metric, called *self-mismatch* probability:

$$s_{self\_mismatch}(x^*) \triangleq 1 - p(m|x^*, x^*) \quad (29)$$

where  $p(m|x_1, x_2) \approx \int p(m|z_1, z_2)p_\theta(z_1|x_1)p_\theta(z_2|x_2)dz_1dz_2$  and  $p(m|z_1, z_2) \triangleq \sigma(-a\|z_1 - z_2\|_2 + b)$  based on their contrastive learning method. Self-mismatch probability can be interpreted as an expectation of the distance between two points randomly sampled from the output distribution. In other words, this uncertainty metric is based on the idea that an input with a large aleatoric uncertainty will span a wider region, resulting in a smaller  $p(m|x, x)$ .

In (Wu and Goodman, 2020), a similar extension is also proposed. The paper introduces a distribution encoder that outputs the representation of Gaussian distribution with diagonal covariance matrix  $\Sigma_\theta(x)$  and extends the normalized temperature-scaled cross-entropy loss (NT-Xent) (Chen et al., 2020a) to distribution-level contrastive objective. The norm of the covariance matrix determined by the distribution encoder is used to assess the reliability of a given input:

$$s_{var}(x^*) \triangleq \|\Sigma_\theta(x^*)\| \quad (30)$$

Despite the benefits of stochastic representation, there are still some shortcomings. One limitation would be that it requires re-training. Large models that have gotten a lot of attention lately are usually trained on a lot of data and are getting bigger, which means they take more time and computing power to train. As a result, it may not always be practical or feasible for users to re-train a model. Additionally, new training schemes can impose unexpected inductive bias to algorithms that are already working well. For example, most probability-based methods are based on standard distributions like the Gaussian or a mixture of them. However, these assumptions may reduce the effectiveness of the model or slow down the training procedure.

### E.2 Novelty Detection in Representation Space

There are several studies that introduce ways to detect out-of-distribution (OOD) samples by determining the novelty of the data representation from a deterministic model (Lee et al., 2018; van Amersfoort et al., 2020; Tack et al., 2020; Mirzae et al., 2022). Although the specific details of

each technique vary, this study observed that these methods commonly use the relative distance information of the query data point’s representation vector to other reference points:

$$s_d(\mathbf{x}^*) \triangleq \text{AvgDist}_k \left( \left\{ \text{dist}(h(\mathbf{x}^*), h(\mathbf{x})) \mid \mathbf{x} \in \mathcal{D}_{\text{ref}} \right\} \right) \quad (31)$$

where  $\text{AvgDist}_k$  outputs an average of the  $k$  smallest relative distances in the representation space between the query  $\mathbf{x}$  and reference points  $\mathcal{D}_{\text{ref}}$ , measured by the distance metric  $\text{dist}$ .

As shown in the table, some works are designed for supervised learning schemes that require instance-specific training labels. [Lee et al. \(2018\)](#) and [van Amersfoort et al. \(2020\)](#) construct reference points by empirical class means:

$$\mathcal{D} = \left\{ \hat{\boldsymbol{\mu}}_c = \frac{1}{N_c} \sum_{\mathbf{x}_i \in \mathcal{D}_{\text{ref}}} h_{\theta}(\mathbf{x}_i) \mathbb{1}(y_i = c) \right\}_{c=1}^C \quad (32)$$

where  $\hat{\boldsymbol{\mu}}_c$  is a centroid of training representations of which the label  $y_i$  is equal to  $c$ ,  $N_c$  is the number of training instances belonging to the label  $c$ , and  $C$  is the number of classes. Then, [Lee et al. \(2018\)](#) defines an uncertainty score as a minimum Mahalanobis distance to each of the centroids using a tied empirical covariance matrix, whereas [van Amersfoort et al. \(2020\)](#) calculates a distance using a Radial Basis Function (RBF) kernel. These approaches can also be viewed as estimating the probability density of the representation to each class.

Nevertheless, the aforementioned methods necessitate training labels, which is not always feasible. In addition, evaluating the uncertainty based on the training labels does not guarantee the method’s efficacy, as downstream tasks frequently use distinct labeling schemes. In order to estimate uncertainty in the absence of class label information, [Tack et al. \(2020\)](#) measures the minimum distance between the query instance and all training instances in the representation space. [Tack et al. \(2020\)](#) additionally suggest to ensemble the uncertainty score with various transformations (i.e., augmentation)  $\mathcal{T}$ :  $s_{d-\text{ens}}(\mathbf{x}^*) = \frac{1}{|\mathcal{T}|} \sum_{t \sim \mathcal{T}} s_d(t(\mathbf{x}^*))$ . Meanwhile, [Mirzae et al. \(2022\)](#) averages the distance to  $k$ -nearest instances rather than taking the closest one to improve the effectiveness.

The main limitation of the above two approaches is the lack of theoretical justification for the proposed metric, as it is founded upon heuristic rules. For example, as demonstrated by our empirical studies in Section 4.2.1, a wrong selection of the distance metric can lead to contradictory results. In addition, as depicted in Figure 2, using a larger  $k$  in those schemes does not necessarily ensure its effectiveness. Considering that the primary goal of these studies is to deploy foundation models in safety-critical settings, establishing a robust reliability measure and analyzing its theoretical validity is vital.